

IGA-based Multi-Index Stochastic Collocation for random PDEs on arbitrary domains

Joakim Beck^a, Lorenzo Tamellini^{b,*}, Raúl Tempone^a

^a*CEMSE, King Abdullah University of Science and Technology (KAUST), Thuwal 23955-6900, Saudi Arabia*

^b*Consiglio Nazionale delle Ricerche - Istituto di Matematica Applicata e Tecnologie Informatiche “E. Magenes” (CNR-IMATI), Via Ferrata 1, 27100, Pavia, Italy*

Abstract

This paper proposes an extension of the Multi-Index Stochastic Collocation method (MISC) for forward Uncertainty Quantification (UQ) problems in computational domains of more generic shapes than a square/cube, by exploiting Isogeometric analysis (IGA) techniques. Introducing IGA solvers within the MISC algorithm is very natural since they are tensor-based PDE solvers, which is precisely what is needed by the MISC machinery; moreover, the combination technique formulation of MISC allows straight-forward reuse of existing implementations of IGA solvers. We present numerical results to showcase the effectiveness of the proposed approach.

Highlights

- Isogeometric solvers used in a Multi-Index Stochastic Collocation framework for forward UQ problems.
- The combination technique formulation of the method allows straight-forward reuse of legacy IGA solvers.

Keywords: Isogeometric analysis, Uncertainty Quantification, Sparse Grids, Stochastic Collocation methods, multilevel methods, combination technique

1. Introduction

Uncertainty Quantification (UQ) has received a considerable amount of attention and is by now considered an essential tool in the domain of Computational Science and Engineering [1, 2, 3]. However, performing UQ analyses still poses a significant computational challenge, since these analyses typically require repeatedly solving the computational model for different values of the uncertain variables of the model. In this paper, we consider in particular models described by (elliptic) PDEs whose solution we denote by \mathbf{u} . Two general “meta-strategies” (complementary to each other) are by now recognized in the UQ community as key to reduce the computational cost and make UQ analyses feasible: a) dimension-adaptivity, i.e., investing more computational cost in approximating the dependence of \mathbf{u} on the random variables whose variability has the largest impact on \mathbf{u} itself, and b) a multi-level approach, in which most of the variability of \mathbf{u} is explored by using “low-fidelity” approximations of the PDE (e.g., coarse meshes, simplified-physics models), and resorting to “high-fidelity” approximations only sparingly. Dimension-adaptivity was the first “meta-strategy” to be introduced in the UQ community and has by now been extensively discussed in the literature, see e.g. in [4, 5, 6, 7], while the multi-level approach is more recent, see e.g. [8, 9, 10].

*Corresponding author

Email addresses: joakim.beck@kaust.edu.sa (Joakim Beck), tamellini@imati.cnr.it (Lorenzo Tamellini), raul.tempone@kaust.edu.sa (Raúl Tempone)

The Multi-Index Stochastic Collocation (MISC) method for random PDEs was first introduced in [11, 12] and represents one attempt to combine both strategies, by proposing a computational algorithm that is able to simultaneously choose the best sequence of computational meshes as well as the random variables whose impact should be more carefully approximated. It is closely related to the sparse-grids technique introduced to solve high-dimensional PDEs [13, 14, 15, 16] and to compute high-dimensional integrals/interpolants [17, 18], and indeed it can be seen as a combination of the two approaches. The main idea behind the algorithm is to write the approximation operator as a linear combination of many less-refined – hence cheaper – approximations (in the spirit of a Richardson extrapolation); in particular, we assign a “profit” to each possible component and eventually include in the computation only those with the largest profit. Another possible approach would be to balance the errors of the physical and stochastic discretizations, as proposed in [19, 20, 21].

Crucially, MISC needs both the physical solver and the sampler in the stochastic domain to have a tensor structure. A tensor construction in the stochastic domain can be obtained by e.g. tensorizing standard Lagrangian (interpolant) polynomials, which would also be the starting point of the classical sparse-grids collocation method for UQ [22, 23]. When it comes to the physical solver, the previous works on MISC [11, 12] only considered square domains over structured grids; [12] only briefly mentioned possible strategies to apply MISC to non-square domains.

In this paper, we extend [11, 12] and consider MISC on arbitrary domains, by resorting to Isogeometric Analysis (IGA) [24, 25]. Isogeometric analysis consists in solving numerically a PDE by approximating its solution with B-splines or Non-Uniform Rational B-Splines (NURBS), i.e., with the same basis employed to parametrize the computational geometry with CAD softwares. The method has attracted considerable attention in the computational science and engineering community, for multiple reasons, including a simpler meshing process and exact domain representation (in some situations), larger flexibility in the choice of the polynomial degree and regularity of the basis, and a more effective error vs. degrees-of-freedom ratio with respect to standard finite element methods; see [26] and references therein. Crucially, multivariate B-splines and NURBS are built by tensorization of univariate B-splines and NURBS, which makes IGA solvers particularly suitable to be used within MISC. It is important to remark that in the end the MISC algorithm will simply prescribe to solve a number of standard uncoupled PDEs, each of them corresponding to a different realization of the random parameters, on physical meshes with different resolution (possibly anisotropic, i.e., more refined along some physical directions). Therefore, previously available IGA software can be readily re-used. We also point out that in the case where there are no random variables, this procedure corresponds to the sparse IGA method for solving PDEs discussed in [27]. Finally, we mention that while IGA is a convenient choice to extend MISC to problems on non-square domains, it is not the only possible choice, and other choices might be envisaged, such as finite differences, finite volumes, \mathbb{Q}_k finite elements; the comparison of these methods per se exceeds the scope of this work.

The rest of this paper is organized as follows. We introduce the general UQ framework for elliptic PDEs with random coefficients Section 2, and discuss IGA solvers in Section 3. We then present the MISC algorithm in Section 4 and showcase the results obtained with MISC on some numerical examples in Section 5. Finally, we draw some conclusions in Section 6.

Throughout the manuscript, we will make extensive use of multi-indices, i.e., vectors with integer components. To this end, we recall here some useful definitions and notations:

- given $\mathbf{i}, \mathbf{j} \in \mathbb{N}^K$, $\mathbf{i} \leq \mathbf{j}$ means that $i_k \leq j_k$ for $k = 1, \dots, K$;
- \mathbf{e}_i is the i -th canonical multi-index, i.e., $(\mathbf{e}_i)_k = 1$ if $i = k$, and zero otherwise;
- $\mathbf{1}$ is a multi-index whose components are all equal to 1;
- given a function $f : \mathbb{R} \rightarrow \mathbb{R}$ and a multi-index \mathbf{i} , $\mathbf{f}(\mathbf{i})$ denotes the multi-index $[f(i_1), f(i_2), \dots, f(i_K)]$;
- a multi-index set $\Lambda \subset \mathbb{N}^K$ is said to be downward closed if

$$\forall \mathbf{i} \in \Lambda, \quad \mathbf{i} - \mathbf{e}_j \in \Lambda \text{ for every } j = 1, \dots, K \text{ such that } \mathbf{i}_j > 1. \quad (1)$$

- the margin of a multi-index set Λ , $\text{Mar}(\Lambda)$, is the set of multi-indices that can be reached “within one step” from Λ ,

$$\text{Mar}(\Lambda) = \{\mathbf{i} \in \mathbb{N}^K \text{ s.t. } \mathbf{i} = \mathbf{j} + \mathbf{e}_k \text{ for some } \mathbf{j} \in \Lambda \text{ and some } k \in \{1, \dots, K\}\}; \quad (2)$$

- the reduced margin of a multi-index set Λ , $\text{Red}(\Lambda)$, is the subset of $\text{Mar}(\Lambda)$ composed by indices from which “every backward step” will take into Λ ,

$$\text{Red}(\Lambda) = \{\mathbf{i} \in \mathbb{N}^K \text{ s.t. } \mathbf{i} - \mathbf{e}_k \in \Lambda \text{ for every } k \in \{1, \dots, K\} \text{ s.t. } i_k > 1\}. \quad (3)$$

2. Problem definition

Let \mathcal{B} be a compact domain in \mathbb{R}^d , $d = 2, 3$, referred to as the “physical domain”. In addition, let $\mathbf{y} = [y_1, y_2, \dots, y_N]$ be an N -dimensional random vector whose components are mutually independent random variables with support $\Gamma_n \subset \mathbb{R}$ and probability density function $\rho_n(y_n)$. Thus, $\mathbf{y} \in \Gamma = \Gamma_1 \times \Gamma_2 \cdots \Gamma_N$; we refer to Γ as the “stochastic domain”, and we can define a probability density function on Γ as $\rho(\mathbf{y}) = \prod_{n=1}^N \rho_n(y_n)$, due to the mutual independence of y_n . Throughout this work, we will often refer to y_n as “stochastic directions”, as a short-hand for “directions of the stochastic domain”.

We consider the following problem: find $\mathbf{u} : \mathcal{B} \times \Gamma \rightarrow \mathbb{R}^m$ such that for ρ -almost every $\mathbf{y} \in \Gamma$,

$$\begin{cases} \mathcal{L}(\mathbf{u}; \mathbf{x}, \mathbf{y}) = \mathcal{F}(\mathbf{x}) & \mathbf{x} \in \mathcal{B}, \\ \mathbf{u}(\mathbf{x}, \mathbf{y}) = 0 & \mathbf{x} \in \partial\mathcal{B}, \end{cases} \quad (4)$$

where \mathcal{L} is a differential operator and \mathcal{F} is an operator on \mathbf{x} . In particular, we will consider in the numerical results section a linear scalar elliptic equation or a linear elasticity equation. We assume well-posedness of the problem in some Hilbert space V for ρ -almost every $\mathbf{y} \in \Gamma$ (specific choices of V will be detailed for each example in Section 5); observe that \mathbf{u} can also be seen as an N -variate Hilbert-space-valued function $\mathbf{u}(\mathbf{y}) : \Gamma \rightarrow V$, and in particular it is convenient to introduce the Bochner space of finite-variance Hilbert-space-valued functions, $L^2_\rho(\Gamma; V) = \{\mathbf{u} : \Gamma \rightarrow V \text{ strongly measurable such that } \int_\Gamma \|\mathbf{u}(\cdot, \mathbf{y})\|_V^2 \rho(\mathbf{y}) d\mathbf{y} < \infty\}$, to which \mathbf{u} is assumed to belong.

The random variables \mathbf{y} model the uncertainties in the system, i.e., account for the fact that coefficients, forcing terms, boundary/initial conditions, and domain shape are often “imperfectly” known, due to measurement errors, lack of data, or intrinsic variability (e.g., wind, rain, earthquakes). The goal of a forward UQ analysis is therefore to assess how much the variability of such random objects affects the quantities of interest of the computation, which could be either the solution \mathbf{u} or a functional thereof. In particular, in this work we assume to be given some functional of the solution \mathbf{u} , $\Phi : V \rightarrow \mathbb{R}$, e.g. $\Phi(\mathbf{v}) = \int_{\mathcal{B}} \mathbf{v}(\mathbf{x}) d\mathbf{x}$ or $\Phi(\mathbf{v}) = \mathbf{v}(\mathbf{x}_0)$, and we aim at estimating its expected value, i.e., we want to compute

$$\mathbb{E}[\Phi(\mathbf{u}(\mathbf{x}, \mathbf{y}))] = \int_\Gamma \Phi(\mathbf{u}(\mathbf{x}, \mathbf{y})) \rho(\mathbf{y}) d\mathbf{y}.$$

In this work we numerically analyze the performance of MISC for this task. This method can also be applicable to more general problems in which the forcing terms, boundary conditions and possibly domain shape are modeled as uncertain. Moreover, we use MISC to select the physical and stochastic discretizations parameters, but other discretization parameters (e.g., time-steps, number of particles, solver tolerances) could be added to the set of parameters governed by MISC. MISC was first introduced in the papers [11, 12], and applied to square domains \mathcal{B} only. The novelty of the present work consists in showing how to extend the MISC methodology to more general physical domain shapes, by replacing the multi-linear Finite Elements solver adopted in those works with the Isogeometric solvers that we present in the next section.

3. Isogeometric solvers

In this section we briefly present the fundamentals of Isogeometric Analysis (IGA) and refer to [24, 25, 26] for a more thorough discussion. The first ingredient of an Isogeometric solver is a B-splines/NURBS representation of the computational domain \mathcal{B} , which is usually provided by a CAD software – we will give some detail on this procedure below. An isogeometric solver will then typically use the same set of basis functions to compute an approximation of the solution of the PDE. Observe however that this is not strictly needed, and one could use two different sets of B-splines/NURBS functions: one to approximate the geometry and another one to approximate the solution.

The B-splines/NURBS representation of $\mathcal{B} \subset \mathbb{R}^d$ consists in a transformation from a reference domain $\widehat{\mathcal{B}}$ (typically, a square or cube) to the physical domain \mathcal{B} , written as a linear combination of B-splines/NURBS functions and so-called control points $\mathbf{P}_i \in \mathbb{R}^d$. Owing to the IGA/CAD literature, we will refer in this work to $\widehat{\mathcal{B}}$ as “parametric domain”.

This construction is based on a tensorization approach (which will be crucial in the following), and therefore we begin our presentation by considering the univariate case. We introduce a reference interval, $\hat{I} = [0, 1]$ and a knot vector over \hat{I} , i.e., a non-decreasing vector $\Xi = [\xi_1, \xi_2, \dots, \xi_{n+p+1}]$, with $n, p \in \mathbb{N}$ and ξ_1, ξ_{n+p+1} coinciding with the extrema of \hat{I} , that will be used to define a set of n B-splines polynomials of degree p over \hat{I} ; observe that Ξ can have repeated entries, for reasons that will be clearer later on. Each ξ_i is called “knot” and an interval (ξ_i, ξ_{i+1}) having non-zero length is an “element”; we denote the number of elements as N_{el} . The elements do not need to have the same length: however, if that is the case, we call such length mesh-size, and denote it by h . Since nodes could have multiplicity greater than one, we define the non-decreasing vector $Z = [\zeta_1, \dots, \zeta_{N_{el}+1}]$ as the vector of knots of Ξ without repetitions, and let m_i be the multiplicity of ζ_i in Ξ , so that $\sum_{i=1}^{N_{el}} m_i = n + p + 1$. A knot vector is said to be open if its first and last knot have multiplicity $p + 1$.

We can now define the B-splines polynomials of degree p on \hat{I} by means of the Cox-De Boor recursive formula: we start with piecewise constant ($\tilde{p} = 0$),

$$\widehat{S}_{i,0}(\xi) = \begin{cases} 1 & \xi_i \leq \xi < \xi_{i+1} \\ 0 & \text{otherwise,} \end{cases} \quad \text{for } i = 1, \dots, n + p$$

and then for $\tilde{p} = 1, \dots, p$ we have the recursive step:

$$\widehat{S}_{i,\tilde{p}}(\xi) = \begin{cases} \frac{\xi - \xi_i}{\xi_{i+\tilde{p}} - \xi_i} \widehat{S}_{i,\tilde{p}-1}(\xi) + \frac{\xi_{i+\tilde{p}+1} - \xi}{\xi_{i+\tilde{p}+1} - \xi_{i+1}} \widehat{S}_{i+1,\tilde{p}-1}(\xi), & \xi_i \leq \xi < \xi_{i+\tilde{p}+1} \\ 0, & \text{otherwise} \end{cases} \quad \text{for } i = 1, \dots, n + p - \tilde{p},$$

with the understanding that $0/0 = 0$; note that if the knot vector Ξ is open, the corresponding basis will be interpolatory in the first and last knot. The B-splines are polynomials of degree p and continuity C^{p-m_i} at ζ_i , which means that one can reduce the regularity of the B-splines by repeating multiple times knots in the knot vector. In particular, repeating a knot p times will result in a basis with C^0 regularity in that knot, which means that the basis will also be interpolatory at that knot; see Figure 1-left for an example. The B-splines generated are linearly independent and we refer to their span as “space of splines”, $W_p(\Xi, \hat{I})$,

$$W_p(\Xi, \hat{I}) = \text{span} \left\{ \widehat{S}_{i,p}, i = 1, \dots, n \right\}.$$

Often, all internal knots are repeated the same number of times, to obtain a B-splines basis with continuity r at each point ζ_i , $0 \leq r \leq p - 1$; if that is the case, we add a superscript r to the notation, i.e., $S_{i,p}^r$ or $W_p^r(\Xi, \hat{I})$. Clearly, for fixed polynomial degree p the number of basis functions n decreases if r increases, see Figure 1-center and right for an example of C_p^{p-1} and C_p^0 B-splines, respectively.

B-splines on d -dimensional domains are defined by tensorization; we discuss here the case $d = 2$, with the understanding that the extension to the case $d = 3$ is trivial. The fact that multivariate B-splines are defined by tensorization is crucial for the development of the MISC methodology, as will become clear in

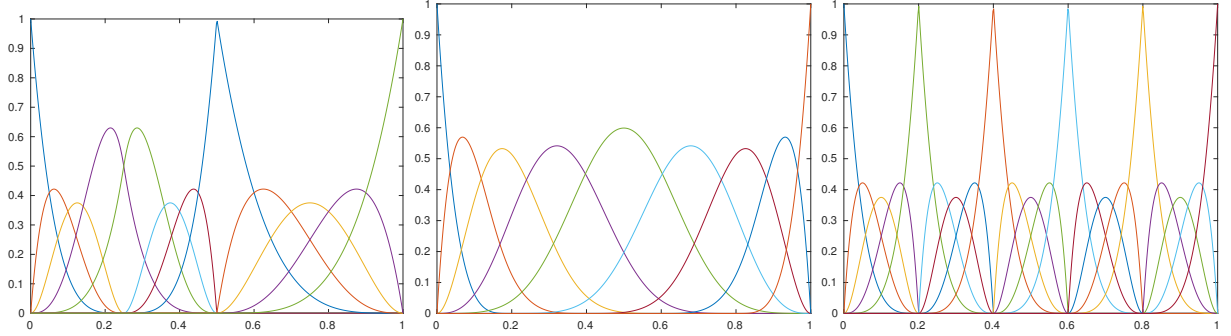


Figure 1: B-splines basis built on different knot-vectors; each knot vector is “open”, i.e., the first and last nodes are repeated $p + 1$ times, with $p = 4$. Left: $\Xi = [0, 0, 0, 0, 0, 0.25, 0.25, 0.25, 0.5, 0.5, 0.5, 0.5, 1, 1, 1, 1]$. Note the different continuity at $\xi = 0.25$ and $\xi = 0.5$ due to different multiplicity: ξ is repeated 3 times, thus the B-splines are C^1 in that knot; ξ is repeated 4 times, thus the B-splines are C^0 in that knot. Center: $\Xi = [0, 0, 0, 0, 0.2, 0.4, 0.6, 0.8, 1, 1, 1, 1]$. In this case, internal knots are repeated only once, resulting in maximally smooth B-splines, i.e., C^3 at the internal knots. Right: $\Xi = [0, 0, 0, 0, 0.2, 0.2, 0.2, 0.2, 0.4, 0.4, 0.4, 0.6, 0.6, 0.6, 0.8, 0.8, 0.8, 0.8, 1, 1, 1, 1]$. Internal knots are repeated p times, resulting in C^0 splines (i.e., Lagrangian Finite Elements of degree p). As expected, the higher the continuity of the basis functions, the smaller the cardinality of the basis.

Section 4. We define the parametric domain $\hat{\mathcal{B}} = \hat{I} \times \hat{I}$ and we consider two open knot vectors Ξ_1, Ξ_2 with $n_1 + p_1 + 1$ and $n_2 + p_2 + 1$ knots, respectively; the corresponding knots without repetitions are denoted by Z_1, Z_2 . We introduce the tensor products $\Xi = \Xi_1 \otimes \Xi_2$ and $\mathbf{Z} = Z_1 \otimes Z_2$; in particular, \mathbf{Z} generates a Cartesian mesh over $\hat{\mathcal{B}}$ composed by $N_{el,1} \times N_{el,2}$ rectangular elements. Owing to the CAD/IGA literature we will refer throughout this work to the two directions ξ_1 and ξ_2 as “parametric directions”. Taking tensor products of the univariate B-splines over Ξ_1 and Ξ_2 we obtain a basis for the space of bi-variate splines

$$W_{\mathbf{p}}^r(\Xi, \hat{\mathcal{B}}) = \text{span}\{\hat{S}_{\mathbf{i}, \mathbf{p}}, \mathbf{i} \leq \mathbf{n}\},$$

where $\mathbf{i} = [i_1, i_2]$, $\mathbf{p} = [p_1, p_2]$, $\mathbf{n} = [n_1, n_2]$, $\mathbf{r} = [r_1, r_2]$, and $\hat{S}_{\mathbf{i}, \mathbf{p}}(\xi_1, \xi_2) = \hat{S}_{i_1, p_1}(\xi_1) \hat{S}_{i_2, p_2}(\xi_2)$.

We are now in the position to introduce the B-splines representation of the computational domain \mathcal{B} as a linear combination of B-splines with given control points $\mathbf{P}_{\mathbf{i}} \in \mathbb{R}^2$ and $\mathbf{i} \leq \mathbf{n}$ (see also Figure 2)

$$\mathbf{x} \in \mathcal{B} \Leftrightarrow \mathbf{x} = \mathbf{G}(\boldsymbol{\xi}) = \sum_{\mathbf{i} \leq \mathbf{n}} \mathbf{P}_{\mathbf{i}} \hat{S}_{\mathbf{i}, \mathbf{p}}(\boldsymbol{\xi}) \text{ for some } \boldsymbol{\xi} \in \hat{\mathcal{B}}.$$

In the CAD literature, the function $\mathbf{G} : \hat{\Omega} \rightarrow \Omega$ is often called parameterization of the geometry \mathcal{B} . Observe that the control points need not belong to \mathcal{B} : this is the case only if the basis is interpolatory in that point, see again Figure 2. With a slight abuse of wording, in the following we will sometimes talk of “physical directions” instead of “parametric directions”, as well as using “physical directions” as a shorthand for the longer “curvilinear coordinates induced by mapping the parametric directions over the physical space”; talking of “physical directions” will be however useful in the juxtaposition with the “stochastic directions” y_1, \dots, y_N .

Non-planar surfaces can be also generated in the same way, by choosing $\mathbf{P}_{\mathbf{i}} \in \mathbb{R}^3$ instead of $\mathbf{P}_{\mathbf{i}} \in \mathbb{R}^2$, see Figure 3-left. A further round of tensorizations, again with $\mathbf{P}_{\mathbf{i}} \in \mathbb{R}^3$, would allow to represent volumetric computational domains \mathcal{B} , see Figure 3-right.

Incidentally, note that many geometries of practical interest, and in particular all conic sections other than parabulae, cannot be represented exactly by B-splines. To this end, the so-called *non-uniform rational B-splines* (NURBS) have been introduced, see again [24, 25, 26] for details. As the name suggests, NURBS are simply ratios of B-splines and most of the properties of B-splines carry on to NURBS.

According to the isogeometric principle, the B-splines basis is also used to approximate the solution of (4). To this end, we introduce the B-splines space on the physical domain \mathcal{B} as follows:

$$W_{\mathbf{p}}(\Xi, \mathcal{B}) = \text{span}\{S_{\mathbf{i}, \mathbf{p}} = \hat{S}_{\mathbf{i}, \mathbf{p}} \circ \mathbf{G}^{-1}, \mathbf{i} \leq \mathbf{n}\}$$

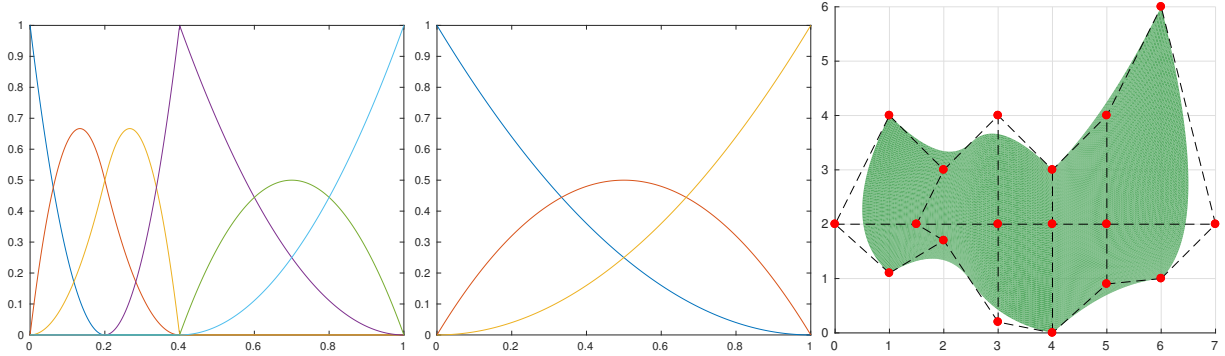


Figure 2: Surfaces are built by linear combinations of control points and tensorized B-splines. Left: B-spline basis along the first reference interval; center: B-spline basis along the second reference interval. The tensor product of these two bases forms the basis (with cardinality 18) for the linear combination used to represent the surface in the right plot. The corresponding 18 control points are marked in red. The dotted lines connecting the control points represent the so-called “control net”.

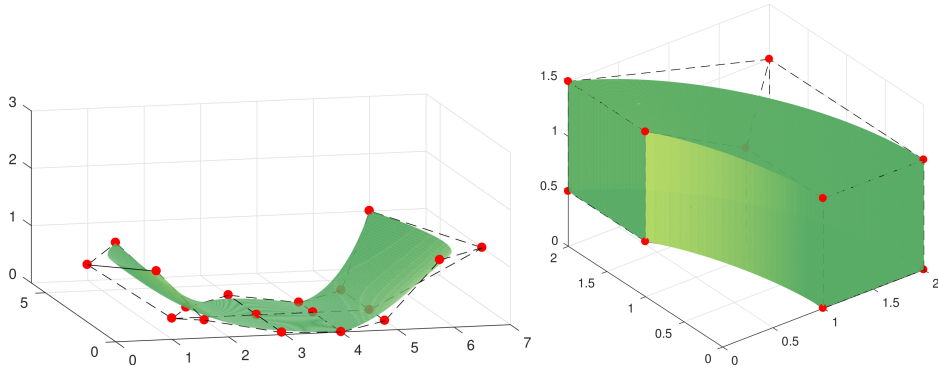


Figure 3: Left: non-planar surface obtained choosing control points in \mathbb{R}^3 instead of \mathbb{R}^2 in the example in Figure 2. Right: volumes can be represented by taking tensor products of three splines bases.

and then approximate the solution of (4) for a fixed value of the random variables $\bar{\mathbf{y}}$ as

$$\mathbf{u}(\mathbf{x}, \bar{\mathbf{y}}) \approx \mathbf{u}_n(\mathbf{x}, \bar{\mathbf{y}}) = \sum_{\mathbf{i} \leq \mathbf{n}} c_{\mathbf{i}} S_{\mathbf{i}, \mathbf{p}}(\mathbf{x}), \quad (5)$$

where the coefficients $c_{\mathbf{i}}$ actually depend on \mathbf{y} but we haven’t shown this dependence for simplicity. The coefficients $c_{\mathbf{i}}$ can be computed by a standard Galerkin approach, or by collocation methods, i.e., inserting (5) in the strong form of the equation, (4), and enforcing that the equation be satisfied in a set of collocation points, which results again in a system of linear equations to be solved [28, 29, 30, 31]. In this work, we employ a standard Galerkin method; we remark again that, as will be clearer later, pre-existing solvers can be readily reused in the context of the MISC method.

Much like with the finite element spaces, the isogeometric approximation of \mathbf{u} in (5), u_n , converges to \mathbf{u} as the cardinality of $W_{\mathbf{p}}(\Xi, \mathcal{B})$ increases, and the convergence results both with respect to h and p are analogous to standard Finite Elements results.

In the following, we fix the polynomial degrees along each parametric direction, i.e., $p_1 = \dots = p_d = p$ and consider h -refinements only, i.e., we will increase the cardinality of the basis by adding knots to the initial knot vectors Ξ_1 and Ξ_2 , but it could be possible to devise a p -MISC technique as well (or a combined $h - p$ version). In particular, for each parametric direction $\xi_i, i = 1, \dots, d$, we will consider a sequence of knot vectors Ξ_i indexed by an integer $\alpha_i \geq 1$, whose number of elements doubles whenever α_i increases by 1, $N_{el, i} \sim 2^{\alpha_i}$. We let $\boldsymbol{\alpha} = [\alpha_1, \dots, \alpha_d] \in \mathbb{N}^d$, and denote the associated solution of the PDE by $\mathbf{u}_{\boldsymbol{\alpha}}$.

4. Multi-Index Stochastic Collocation (MISC)

Besides IGA, the other basic building block of MISC is a tensorized quadrature formula over the stochastic domain Γ , that can be used to evaluate e.g. expected value, variance and higher-order moments of multi-variate random functions defined over Γ .

Let us therefore start by introducing a quadrature operator for a univariate real-valued continuous function $v(t) : \tilde{\Gamma} \rightarrow \mathbb{R}$, with the understanding that $\tilde{\Gamma}$ is a placeholder for any of the univariate sub-domains $\Gamma_1, \dots, \Gamma_N$ composing the random space $\Gamma = \Gamma_1 \times \dots \times \Gamma_N$; therefore, it comes with an associate probability density function, that we denote by $\tilde{\rho}$. The quadrature operator is defined as

$$\mathcal{Q}^{m(\beta)} : C^0(\tilde{\Gamma}) \rightarrow \mathbb{R}, \quad \mathcal{Q}^{m(\beta)}[v] = \sum_{j=1}^{m(\beta)} v(t_{\beta,j}) \omega_{\beta,j},$$

where $\beta \geq 1$ is a positive integer (usually referred to as the “refinement level” or just “level” of the quadrature operator), $m(\beta)$ a strictly increasing function giving the number of distinct quadrature points to be used, $\{t_{\beta,j}\}_{j=1}^{m(\beta)} \subset \tilde{\Gamma}$, with corresponding weights $\{\omega_{\beta,j}\}_{j=1}^{m(\beta)}$. The quadrature points should be chosen according to the underlying probability measure $\tilde{\rho}$, see e.g. [5, 32]. Moreover, it is advantageous if the quadrature points are chosen to be “nested”, i.e., $\{t_{\beta,j}\}_{j=1}^{m(\beta)} \subset \{t_{\beta+1,j}\}_{j=1}^{m(\beta+1)}, \forall \beta \geq 1$; in the numerical examples of this work we will consider problems depending on uniform random variables, for which a number of different families of nested quadrature points exist: the Clenshaw–Curtis points, several variants of the Leja points, and the Gauss–Patterson points, see e.g. [5, 33, 34, 35, 36]. In particular, we adopt the Clenshaw–Curtis points, which are defined as

$$t_{\beta,j} = \cos\left(\frac{(j-1)\pi}{m(\beta)-1}\right), \quad 1 \leq j \leq m(\beta),$$

and are therefore nested provided that the function $m(\beta)$ is chosen as

$$m(0) = 0, \quad m(1) = 1, \quad m(\beta) = 2^{\beta-1} + 1, \quad \beta \geq 2.$$

The extension to multi-variate real-valued continuous functions $v(\mathbf{t}) : \Gamma \rightarrow \mathbb{R}$ is obtained by tensorization of the univariate quadrature operators. In detail, we introduce a multi-index $\boldsymbol{\beta} \in \mathbb{N}^N$, whose i -th component gives the level of the univariate quadrature to be used along Γ_i , and define the multi-variate quadrature operator as

$$\mathcal{Q}^{m(\boldsymbol{\beta})} : C^0(\Gamma) \rightarrow \mathbb{R}, \quad \mathcal{Q}^{m(\boldsymbol{\beta})} = \bigotimes_{1 \leq i \leq N} \mathcal{Q}^{m(\beta_i)}, \quad \mathcal{Q}^{m(\boldsymbol{\beta})}[v] = \sum_{j=1}^{\#\mathbf{m}(\boldsymbol{\beta})} v(\mathbf{t}_j) \omega_j,$$

where \mathbf{t}_j are points in the Cartesian grid $\bigotimes_{1 \leq i \leq N} \{z_{\beta_i,j}\}_{j=1}^{m(\beta_i)}$, ω_j are the corresponding products of weights of the one-dimensional quadrature rules, and $\#\mathbf{m}(\boldsymbol{\beta})$ denotes the total number of quadrature points in the Cartesian grid, $\#\mathbf{m}(\boldsymbol{\beta}) = \prod_{i=1}^N m(\beta_i)$.

We are now in the position to introduce the MISC approximation of the expected value of functionals of the solution of the PDE at hand, $\mathbb{E}[\Phi(\mathbf{u}(\mathbf{x}, \mathbf{y}))]$. For ease of presentation, we introduce the function $\phi : \Gamma \rightarrow \mathbb{R}$ that associates to each \mathbf{y} the corresponding value of the functional $\phi(\mathbf{y}) = \Phi(\mathbf{u}(\mathbf{x}, \mathbf{y}))$, so that our goal becomes computing an approximation of $\mathbb{E}[\phi(\mathbf{y})]$.

Clearly, the value of $\phi(\mathbf{y})$ is accessible to us only by solving the PDE at hand upon fixing the value of the random vector \mathbf{y} : in particular, we denote by $\phi_{\boldsymbol{\alpha}}$ the value of ϕ obtained by post-process of $\mathbf{u}_{\boldsymbol{\alpha}}$, where as already mentioned $\boldsymbol{\alpha}$ prescribes the number of elements in the knot vectors used to build the IGA solver, $N_{el,i} \sim 2^{\alpha_i}$.

The fully discrete approximation of $\mathbb{E}[\phi(\mathbf{y})]$ is therefore completely determined upon choosing the discretizations $\boldsymbol{\alpha}$ in the physical space and by $\boldsymbol{\beta}$ in the probability space, i.e., $\mathbb{E}[\phi(\mathbf{y})] \approx M_{\boldsymbol{\alpha}, \boldsymbol{\beta}} = \mathcal{Q}^{m(\boldsymbol{\beta})}[\phi_{\boldsymbol{\alpha}}]$. Of course, an ideal approximation $M_{\boldsymbol{\alpha}, \boldsymbol{\beta}}$ would be obtained by setting $\alpha_1 = \dots = \alpha_d = \bar{\alpha} \gg 1$ and $\beta_1 = \dots = \beta_N = \bar{\beta} \gg 1$, which is however out of computational reach for even moderate values of $d, N, \bar{\alpha}, \bar{\beta}$,

due to its combinatorial computational cost. Thus, we resort in MISC to the classical “sparsification” construction, already introduced in literature for solving high-dimensional PDEs [14] and quadrature problems [17].

To this end, we need to introduce the so-called univariate and multivariate “detail operators” on the physical and stochastic domain as follows, with the understanding that $M_{\alpha,\beta} = 0$ as soon as at least one component of α or β is zero:

$$\begin{aligned}
\text{Univariate physical detail:} \quad & \Delta_i^{\text{phys}}[M_{\alpha,\beta}] = M_{\alpha,\beta} - M_{\alpha-e_i,\beta} \text{ with } 1 \leq i \leq d; \\
\text{Univariate stochastic detail:} \quad & \Delta_i^{\text{stoc}}[M_{\alpha,\beta}] = M_{\alpha,\beta} - M_{\alpha,\beta-e_i} \text{ with } 1 \leq i \leq N; \\
\text{Multivariate physical detail:} \quad & \Delta^{\text{phys}}[M_{\alpha,\beta}] = \bigotimes_{i=1}^d \Delta_i^{\text{phys}}[M_{\alpha,\beta}]; \\
\text{Multivariate stochastic detail:} \quad & \Delta^{\text{stoc}}[M_{\alpha,\beta}] = \bigotimes_{j=1}^N \Delta_j^{\text{stoc}}[M_{\alpha,\beta}]; \\
\text{Mixed multivariate detail:} \quad & \Delta^{\text{mix}}[M_{\alpha,\beta}] = \Delta^{\text{stoc}}[\Delta^{\text{phys}}[M_{\alpha,\beta}]].
\end{aligned}$$

Observe that taking tensor products of univariate details amounts to composing their actions, e.g.,

$$\Delta^{\text{phys}}[M_{\alpha,\beta}] = \bigotimes_{i=1}^d \Delta_i^{\text{phys}}[M_{\alpha,\beta}] = \Delta_1^{\text{phys}} \left[\Delta_2^{\text{phys}} \left[\dots \Delta_d^{\text{phys}} [M_{\alpha,\beta}] \right] \right],$$

and analogously for the stochastic multivariate detail operators, $\Delta^{\text{stoc}}[M_{\alpha,\beta}]$. Crucially, this in turn implies that the evaluating the multivariate operators can be performed by evaluating certain full-tensor approximations $M_{\alpha,\beta}$ and then taking linear combinations:

$$\begin{aligned}
\Delta^{\text{phys}}[M_{\alpha,\beta}] &= \Delta_1^{\text{phys}} \left[\Delta_2^{\text{phys}} \left[\dots \Delta_D^{\text{phys}} [M_{\alpha,\beta}] \right] \right] = \sum_{\mathbf{j} \in \{0,1\}^d} (-1)^{|\mathbf{j}|} M_{\alpha-\mathbf{j},\beta}; \\
\Delta^{\text{stoc}}[M_{\alpha,\beta}] &= \sum_{\mathbf{j} \in \{0,1\}^N} (-1)^{|\mathbf{j}|} M_{\alpha,\beta-\mathbf{j}}.
\end{aligned}$$

The latter expression is known in the sparse-grids community as “combination technique”, and can be very useful for a practical implementations of the method, especially for evaluating $\Delta^{\text{phys}}[M_{\alpha,\beta}]$: indeed, it allows to evaluate detail operators by calling up to 2^d times pre-existing softwares on different meshes (in this case, IGA solvers) in a “black-box” fashion. As an example, if $d = 2$, one has

$$\begin{aligned}
\Delta^{\text{phys}}[M_{\alpha,\beta}] &= \Delta_2^{\text{phys}} \left[\Delta_1^{\text{phys}} [M_{\alpha,\beta}] \right] \\
&= \Delta_2^{\text{phys}} [M_{\alpha,\beta} - M_{\alpha-e_1,\beta}] \\
&= M_{\alpha,\beta} - M_{\alpha-e_1,\beta} - M_{\alpha-e_2,\beta} + M_{\alpha-1,\beta}.
\end{aligned}$$

We remark that the four meshes needed to evaluate the combination technique expression above are possibly anisotropic, i.e., with different levels of discretization along the different physical directions. A similar expression holds for the stochastic details, as well as for the mixed details: in particular, evaluating $\Delta^{\text{stoc}}[M_{\alpha,\beta}]$ requires evaluating up to 2^N operators $M_{\alpha,\beta}$ over different quadrature grids, and evaluating $\Delta^{\text{mix}}[M_{\alpha,\beta}]$ requires evaluating up to 2^{d+N} operators $M_{\alpha,\beta}$ over different quadrature grids and physical meshes. For instance, if $d = N = 2$,

$$\Delta^{\text{stoc}}[M_{\alpha,\beta}] = M_{\alpha,\beta} - M_{\alpha-e_1,\beta} - M_{\alpha-e_2,\beta} + M_{\alpha-1,\beta};$$

$$\begin{aligned}
\Delta^{\text{mix}}[M_{\alpha,\beta}] &= \Delta^{\text{stoc}}[\Delta^{\text{phys}}[M_{\alpha,\beta}]] \\
&= \Delta^{\text{stoc}}[M_{\alpha,\beta} - M_{\alpha-e_1,\beta} - M_{\alpha-e_2,\beta} + M_{\alpha-1,\beta}] \\
&= M_{\alpha,\beta} - M_{\alpha-e_1,\beta} - M_{\alpha-e_2,\beta} + M_{\alpha-1,\beta} \\
&\quad - (M_{\alpha,\beta-e_1} - M_{\alpha-e_1,\beta-e_1} - M_{\alpha-e_2,\beta-e_1} + M_{\alpha-1,\beta-e_1}) \\
&\quad - (M_{\alpha,\beta-e_2} - M_{\alpha-e_1,\beta-e_2} - M_{\alpha-e_2,\beta-e_2} + M_{\alpha-1,\beta-e_2}) \\
&\quad + M_{\alpha,\beta-1} - M_{\alpha-e_1,\beta-1} - M_{\alpha-e_2,\beta-1} + M_{\alpha-1,\beta-1}.
\end{aligned}$$

Observe that by introducing these operators we have access to a hierarchical decomposition of $M_{\alpha,\beta}$: indeed, the following is a telescopic identity

$$M_{\alpha,\beta} = \sum_{[i,j] \leq [\alpha,\beta]} \Delta^{\text{mix}}[M_{i,j}],$$

i.e., it can be easily verified by replacing each term $\Delta^{\text{mix}}[M_{i,j}]$ with the the corresponding combination technique formula that all terms but $M_{\alpha,\beta}$ will cancel. For instance, if $d = N = 1$, recalling that by definition $M_{i,j} = 0$ if either $i = 0$ or $j = 0$, we have

$$\begin{aligned}
\sum_{[i,j] \leq [2,2]} \Delta^{\text{mix}}[M_{i,j}] &= \Delta^{\text{mix}}[M_{1,1}] + \Delta^{\text{mix}}[M_{1,2}] + \Delta^{\text{mix}}[M_{2,1}] + \Delta^{\text{mix}}[M_{2,2}] \\
&= M_{1,1} + (M_{1,2} - M_{1,1}) + (M_{2,1} - M_{1,1}) + M_{2,2} - M_{2,1} - M_{1,2} - M_{1,1} \\
&= M_{2,2}.
\end{aligned} \tag{6}$$

The crucial observation is that (under suitable regularity assumptions on \mathbf{u}), not all of the details in the above hierarchical decomposition contribute equally to the approximation, i.e., they can be discarded and the resulting formula will retain good approximation properties for a fraction of the computational cost. Thus, we introduce the MISC approximation of $\mathbb{E}[\phi]$ as

$$\mathcal{I}_{\Lambda}^{\text{MISC}} = \sum_{[\alpha,\beta] \in \Lambda} \Delta^{\text{mix}}[M_{\alpha,\beta}],$$

for a suitable multi-index set $\Lambda \subset \mathbb{N}^{d+N}$, which should be chosen as downward closed, cf. (1). Clearly, also the MISC estimator has a combination technique expression, which can be written in compact form as

$$\mathcal{I}_{\Lambda}^{\text{MISC}} = \sum_{[\alpha,\beta] \in \Lambda} \Delta^{\text{mix}}[M_{\alpha,\beta}] = \sum_{[\alpha,\beta] \in \Lambda} \sum_{\substack{[i,j] \in \{0,1\}^{d+N} \\ [\alpha+i,\beta+j] \in \Lambda}} (-1)^{|[i,j]|} M_{\alpha,\beta}, \tag{7}$$

which means that again we can evaluate MISC by evaluating independently full-tensor operators $M_{\alpha,\beta}$ and combining them linearly according to (7).

Of course, the effectiveness of the MISC estimator depends on the choice of the multi-index set Λ ; the general principle underlying the “sparse” construction is that Λ should be chosen to exclude from the estimate isotropic full-tensor operators, i.e., operators which simultaneously refine both the mesh on the physical domain and the quadrature grid on the stochastic domain. One should rather opt for indices that refine only a subset of physical and/or stochastic directions, and then use the combination technique formula to combine the partial results; this general idea is exemplified in Figure 4. In a sense, the sparsification approach can be ascribed to the family of Richardson extrapolation methods, by which one considers an ensemble of coarse approximations and combines in such a way that the result is more accurate than each of the components alone. A simple yet quite effective choice of Λ that prunes full-tensor operators is the so-called “total-degree” set [14, 37]

$$\Lambda_{TD}(\boldsymbol{\kappa}, \mathbf{g}, w) = \left\{ [\alpha, \beta] \in \mathbb{N}^{d+N} : \sum_{i=1}^d \kappa_i \alpha_i + \sum_{i=1}^N g_i \beta_i \leq w \right\}, \text{ for some } w \in \mathbb{N}, \tag{8}$$

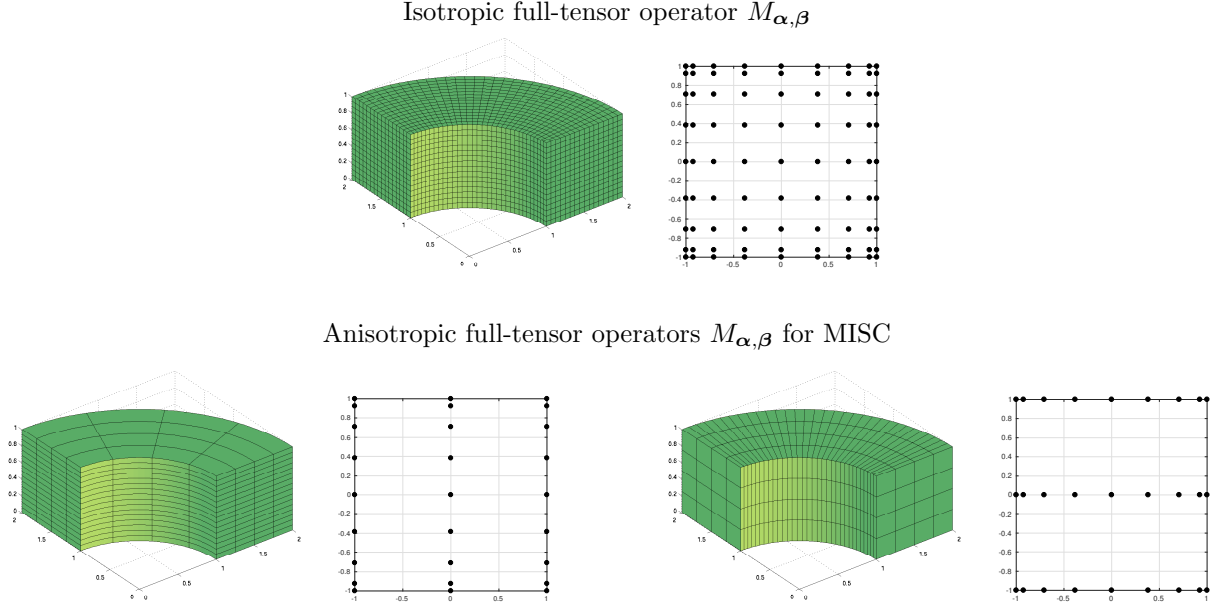


Figure 4: A full-tensor method would require sampling the stochastic domain with an isotropic Cartesian grid, and solving for each sample the PDE on a mesh refined along all physical directions, see top row. Instead, the MISC method requires that the stochastic domain be sampled with anisotropic Cartesian grids, and the PDE be solved on anisotropic meshes in space, which are combined in such a way that not all physical and stochastic directions are simultaneously refined: some meshes satisfying this principle are shown in the second and third row. The results need to be linearly combined, according the combination technique formula in (7).

where κ_i, g_i are positive real values that can be used to allow more refinement along selected physical and/or stochastic directions (the smaller the coefficient, the larger the maximum refinement level allowed along that specific direction). For instance, if $d = N = 1, w = 2$ and the weights are chosen as $\kappa_i, g_i = 1$, we have the set $\Lambda_{TD}(1, 1, 2) = \{[i, j] \in \mathbb{N}^2 : i + j \leq 2\}$, which amounts to

$$\begin{aligned}
 \sum_{[i,j] \in \Lambda_{TD}(1,1,2)} \Delta^{\text{mix}}[M_{i,j}] &= \Delta^{\text{mix}}[M_{1,1}] + \Delta^{\text{mix}}[M_{1,2}] + \Delta^{\text{mix}}[M_{2,1}] \\
 &= M_{1,1} + (M_{1,2} - M_{1,1}) + (M_{2,1} - M_{1,1}) \\
 &= M_{1,2} + M_{2,1} - M_{1,1}.
 \end{aligned}$$

A similar choice of set Λ , i.e., total-degree sets with all weights set to 1, was advocated also in [38, 21]. The last expression should be contrasted with (6), and shows that the most refined operator $M_{2,2}$ is no longer to be computed. To devise an optimal strategy for selecting a good multi-index set, we introduce this error decomposition:

$$\begin{aligned}
 |\mathbb{E}[\phi] - \mathcal{I}_\Lambda^{\text{MISC}}| &= \left| \mathbb{E}[\phi] - \sum_{[\alpha,\beta] \in \Lambda} \Delta^{\text{mix}}[M_{\alpha,\beta}] \right| \\
 &= \left| \sum_{[\alpha,\beta] \notin \Lambda} \Delta^{\text{mix}}[M_{\alpha,\beta}] \right| \leq \sum_{[\alpha,\beta] \notin \Lambda} |\Delta^{\text{mix}}[M_{\alpha,\beta}]| \leq \sum_{[\alpha,\beta] \notin \Lambda} E_{\alpha,\beta}, \quad (9)
 \end{aligned}$$

where we have defined $E_{\alpha,\beta} = |\Delta^{\text{mix}}[M_{\alpha,\beta}]|$; $E_{\alpha,\beta}$ thus represents the “error contribution” of $[\alpha, \beta]$, i.e., the reduction in the approximation error due to having added $[\alpha, \beta]$ to the current index-set Λ . Similarly, we define the “work contribution” $W_{\alpha,\beta}$ as the work required to add $[\alpha, \beta]$ to the current index-set Λ , for instance, summing the degrees of freedom of all the new PDEs that need to be evaluated due to the addition of $[\alpha, \beta]$. Thus, it can be easily seen the strategy that delivers the best choice of Λ consists in adding to Λ

only the set of multi-indices with the largest profit $P_{\alpha,\beta} = \frac{E_{\alpha,\beta}}{W_{\alpha,\beta}}$ [11, 12]:

$$\Lambda_\epsilon = \left\{ [\alpha, \beta] \in \mathbb{N}^{d+N} : \frac{E_{\alpha,\beta}}{W_{\alpha,\beta}} \geq \epsilon \right\}, \text{ for some } \epsilon > 0. \quad (10)$$

Such set can be determined by classic adaptive algorithms such as those discussed in [39, 40, 41] for quadrature problems, or according to a-priori bounds on the size of $E_{\alpha,\beta}$, $W_{\alpha,\beta}$; in this work, we consider the latter approach. In particular, all the problems that will be considered in the numerical sections consist of elliptic PDE, for which an expression for the optimal Λ was derived in [11], under the assumptions that the problem depends on uniform random variables and that the univariate quadrature operator used on the stochastic domain is built over Clenshaw–Curtis points. In details, for some positive real values $r_i, c_i, i = 1 \dots, d$ and $g_j, j = 1 \dots, N$ that we will define in a moment, [11] proved that the following estimates are good:

$$E_{\alpha,\beta} = \mathcal{O}(\tilde{E}_{\alpha,\beta}), \quad \tilde{E}_{\alpha,\beta} = 2^{-\sum_{i=1}^d \alpha_i r_i - \sum_{i=1}^N g_i 2^{\beta_i} \log_2 e}, \quad (11)$$

$$W_{\alpha,\beta} = \mathcal{O}(\tilde{W}_{\alpha,\beta}), \quad \tilde{W}_{\alpha,\beta} = 2^{\sum_{i=1}^d \alpha_i c_i + \sum_{i=1}^N \beta_i}, \quad (12)$$

so that a good estimate of (10) is

$$\Lambda_{OP}(\mathbf{r}, \mathbf{c}, \mathbf{g}, w) = \left\{ [\alpha, \beta] \in \mathbb{N}^{d+N} : \sum_{i=1}^d (r_i + c_i) \alpha_i + \sum_{i=1}^N (\beta_i + g_i 2^{\beta_i} \log_2 e) \leq w \right\}, \text{ for some } w \in \mathbb{N}, \quad (13)$$

which is reminiscent of the total-degree set (8). The coefficients $r_i, c_i, i = 1 \dots, d$ and $g_j, j = 1 \dots, N$ are defined as follows, and can either be determined a-priori or learnt during the execution of the MISC algorithm:

- r_1, \dots, r_d are the h -convergence rates of the PDE solver for the approximation of $\phi(\mathbf{y})$ for fixed \mathbf{y} , i.e., the rates in this estimate,

$$|\phi_{\alpha}(\mathbf{y}) - \phi(\mathbf{y})| \leq C \prod_{i=1}^d N_{el,i}^{-r_i} = C \prod_{i=1}^d 2^{-\alpha_i r_i}. \quad (14)$$

α_i can be determined a-priori by standard finite element theory, keeping into account possible corner/edge singularities as well as possible grading of meshes that could be introduced to mitigate the effects of such singularities, cf. e.g. [42, 43]; however, as already mentioned, we will content ourselves with measuring r_i numerically.

- c_1, \dots, c_d are the rates of the increase of the cost of computing the approximation of $\phi(\mathbf{y})$ for fixed \mathbf{y} as the physical mesh becomes finer,

$$\text{cost}[\phi_{\alpha}(\mathbf{y})] \leq C \prod_{i=1}^d 2^{\alpha_i c_i}. \quad (15)$$

This cost is dominated by assembling and solving the linear system, since evaluating linear functionals of the solution is typically very cheap (e.g., a matrix-vector multiplication). We mention in-passing that relating the cost of assembling and solving the IGA linear system to the number of degrees of freedom is a delicate operation, see e.g. [44]; we will content ourselves with fitting these rates from numerical experiments.

- g_1, \dots, g_N are the decay rates of the following bound on coefficients of the multivariate Legendre expansion of $\phi(\mathbf{y})$:

$$\phi(\mathbf{y}) = \sum_{\mathbf{i} \in \mathbb{N}^N} \hat{\phi}_{\mathbf{i}} \mathcal{L}_{\mathbf{i}}(\mathbf{y}), \quad |\hat{\phi}_{\mathbf{i}}| \leq C e^{-\sum_{n=1}^N g_n i_n}.$$

Algorithm 1: MISC implementation

Multi Index Stochastic Collocation($r_1, \dots, r_d, c_1, \dots, c_d, w_0, TOL$)

```

 $\Lambda = \Lambda_{TD}(\mathbf{1}, \mathbf{1}, w_0)$  ;
Compute MISC estimate  $\mathcal{I}_\Lambda^{\text{MISC}}$  as in (7) ;
Least squares fit of rates  $g_i$  in (11) with  $E_{\alpha, \beta}$  for  $[\alpha, \beta] \in \Lambda$  ;
Compute  $\tilde{E}_{\alpha, \beta}, \tilde{W}_{\alpha, \beta}$  as in (11), (12), and  $\tilde{P}_{\alpha, \beta} = \tilde{E}_{\alpha, \beta} / \tilde{W}_{\alpha, \beta}$  for  $[\alpha, \beta] \in \text{Mar}(\Lambda)$  ;
while  $\sum_{[\alpha, \beta] \in \text{Mar}(\Lambda)} \tilde{E}_{\alpha, \beta} > TOL$  do
   $\Theta = \left\{ [\alpha, \beta] \in \text{Red}(\Lambda) : \tilde{P}_{\alpha, \beta} = \max_{[\alpha, \beta] \in \text{Red}(\Lambda)} \{ \tilde{P}_{\alpha, \beta} \} \right\}$  ;
   $\Lambda = \Lambda \cup \Theta$  ;
  Compute MISC estimate  $\mathcal{I}_\Lambda^{\text{MISC}}$  as in (7) ;
  Least squares fit of rates  $g_i$  in (11) with  $E_{\alpha, \beta}$  for  $[\alpha, \beta] \in \Lambda$  ;
  Compute  $\tilde{E}_{\alpha, \beta}, \tilde{W}_{\alpha, \beta}$  as in (11), (12), and  $\tilde{P}_{\alpha, \beta} = \tilde{E}_{\alpha, \beta} / \tilde{W}_{\alpha, \beta}$  for  $[\alpha, \beta] \in \text{Mar}(\Lambda)$  ;
end
end

```

In practice, we use the implementation reported in Algorithm 1. The stopping criterion in Algorithm 1 above consists in checking that the sum of the error contribution in the margin of the index set Λ , cf. (2), is smaller than the required tolerance,

$$\sum_{[\alpha, \beta] \in \text{Mar}(\Lambda)} E_{\alpha, \beta} < \text{TOL}. \quad (16)$$

This choice is motivated by the error decomposition in (9), where we further approximate the error bound by

$$|\mathbb{E}[\Phi(u)] - \mathcal{I}^{\text{MISC}}(u)| \leq \sum_{[\alpha, \beta] \notin \Lambda} E_{\alpha, \beta} \approx \sum_{[\alpha, \beta] \in \text{Mar}(\Lambda)} \tilde{E}_{\alpha, \beta}.$$

The approximation is reasonable only if the size of the details $E_{\alpha, \beta}$ decreases quickly enough (which is true under sufficient smoothness hypotheses for the problem at hand both with respect to the physical variables and the random variables), see e.g. [45].

5. Numerical results

In this section, we illustrate the performance of the MISC methodology by some numerical examples. The random variables are considered to be uniformly distributed, and therefore we will employ Clenshaw–Curtis quadrature points for the approximation over the stochastic space. Computational times shown have been recorded on single-core runs of MISC on a workstation equipped with Intel Xeon E5 processors with clock rate 2.8 GHz and Ubuntu 16.04 operative system. The IGA solver used is provided by the Matlab/Octave package GeoPDEs, available at <http://rafavzqz.github.io/geopdes/>, see also [46].

5.1. Test 1 - 3d linear elliptic PDE with random diffusion coefficient

In this test we consider a classic UQ benchmark, i.e., a linear elliptic PDE with random diffusion coefficient, for which a vast body of literature exist, cf. e.g. [22, 47] and references therein,

$$\begin{cases} -\text{div}[a(\mathbf{x}, \mathbf{y}) \nabla u(\mathbf{x}, \mathbf{y})] = 1 & \mathbf{x} \in \mathcal{B}, \\ u(\mathbf{x}, \mathbf{y}) = 0 & \mathbf{x} \in \partial \mathcal{B}. \end{cases}$$

We consider as physical domain the thick quarter of ring in Figure 5-top-left, which is a typical benchmark geometry in the IGA literature; the random vector \mathbf{y} is composed by $N = 3$ i.i.d. uniform random variables,

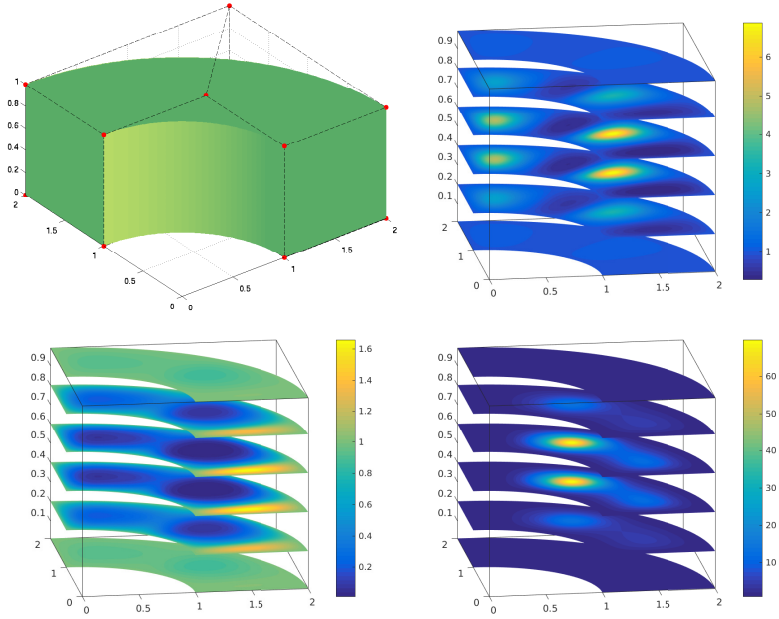


Figure 5: Test 1. Computational domain (top-left) and three different realizations of the random field.

$y_i \sim \mathcal{U}(-1, 1)$, i.e., $\Gamma = [-1, 1]^3$. The random field $a(\mathbf{x}, \mathbf{y})$ models variability in the properties of the material, e.g. uneven heat capacity due to imperfections. Because of the peculiar shape of the computational domain, we express the random field in cylindrical coordinates as

$$\begin{aligned}
 a([\rho, \theta, z], \mathbf{y}) &= e^{c \gamma([\rho, \theta, z], \mathbf{y})}, \quad \text{with } c = 4 \text{ and} \\
 \gamma([\rho, \theta, z], \mathbf{y}) &= y_1 \sin(2\theta) \sin(\pi(\rho - 1)) \sin(\pi z) + \\
 &\quad 0.4 y_2 \sin(8\theta) \sin(\pi(\rho - 1)) \sin(\pi z) + \\
 &\quad 0.1 y_3 \sin(16\theta) \sin(\pi(\rho - 1)) \sin(\pi z).
 \end{aligned}$$

The expression for $\gamma([\rho, \theta, z], \mathbf{y})$ mimics the expression that one would obtain by applying a spectral decomposition like Fourier [48] or Karhunen–Loève [49] to a random field and then truncating it to retain only the most important modes. Three different realizations of the random field can be seen in Figure 5. Note the different scales of the point-wise values of the realizations (due to the magnifying effect of the exponential operation in the definition of the random field), as well as the difference in the frequencies of oscillations. By construction, there exist two real values $0 < m < M$ such that $m < a([\rho, \theta, z], \mathbf{y}) < M$ for ρ -almost every $\mathbf{y} \in \Gamma$, which guarantees that the problem is well-posed in $V = H_0^1(\mathcal{B})$, and that there exists an optimally convergent approximation of u in $L_\rho^2(\Gamma; V)$ as well as $L_\rho^\infty(\Gamma; V)$ based either on ρ -orthonormal polynomials or on interpolation processes, see e.g. [5, 50]. We are interested in computing the expected value of the integral of the solution over the physical domain, $\Phi(\mathbf{v}) = \int_{\mathcal{B}} \mathbf{v}(\mathbf{x}, \cdot) d\mathbf{x}, \forall \mathbf{v} \in V$.

Concerning the IGA solver, note that the computational domain in this example cannot be described exactly by B-splines, being some edges arcs of circles. Therefore, as already pointed out in Section 3, we resort to using NURBS basis functions instead of B-splines, which however does not imply any change in the MISC procedure. Specifically, we employ NURBS of degree $p = 2$ and maximal continuity, C^1 ; incidentally, note that this means that a degree-elevation operation (i.e., p -refinement) will have to be performed preliminary to actually starting the MISC computation, since the thick quarter of annulus geometry is defined by linear polynomials in two out of three parametric directions. The knots in the parametric domain are not uniform, but rather scaled towards the edges of the domain with a power law with exponent set to 3 to capture the edge singularities of the IGA solver for fixed \mathbf{y} , and thus improve the convergence of the solution as the

mesh-size decreases; the specific choice of the exponent has been found by a numerical exploration aimed at recovering the optimal convergence of the IGA solver on analogous problems (albeit without randomness), see [27] and references therein for more details. For a fixed realization of the random field, the Galerkin stiffness matrix for B-splines and NURBS is typically less sparse than when using Finite Element (due to the larger support of B-splines/NURBS, which is proportional to the degree p , [44]), so we employ a direct solver (Matlab’s backslash).

We will compare the convergence results of MISC with two different multi-level methods, namely, the Multi-Level Monte Carlo (MLMC, [8]) in the implementation proposed in [51], and its refined version Multi-Index Monte Carlo (MIMC, [9]).

The convergence of MLMC and MIMC for elliptic PDEs with random coefficients has been discussed respectively in [8] and in [9] and depends on the rates r_i, c_i in (14) and (15), respectively. We have found numerically that r_i, c_i have approximate values $r_i = [4, 4, 4], c_i = [1, 1, 1]$, which implies that the computational cost for reaching an accuracy TOL is expected to be $\mathcal{O}(\text{TOL}^{-2})$ for both MLMC and MIMC, see [8, 9] for details; this is the optimal rate for sampling schemes, i.e., most of the sampling is done on the coarsest mesh levels, such that the computational cost is “equivalent to sampling a random variable” (of course, up to the cost of solving the linear system corresponding to the coarsest levels, which is still non-negligible). The cost of a standard Monte Carlo analysis where for an assigned tolerance TOL we choose a physical mesh and a number of samples in the stochastic domain such that both the deterministic and statistical errors are smaller than TOL/2 would instead be proportional to $\mathcal{O}(\text{TOL}^{-2.75})$, see e.g. [8].

Concerning MISC, convergence results are available in [11] for the case of a PDE depending on finitely many random variables (as is the case in the current example) and in [12] for the case of a PDE depending on a countable sequence of random variables. The convergence result for finitely many random variables in [11] depends on the rates r_i, c_i only, i.e., g_i do not play any role; in other words, the approximation over the probability space by tensorized quadrature is expected to converge fast enough that it should not impact the overall convergence rate. More precisely, the result in [11] predicts for the a-priori chosen set in (13) the asymptotic convergence estimate

$$|\mathbb{E}[\Phi(u)] - \mathcal{I}^{\text{MISC}}(u)| \leq C \text{Work}^{-4} (\log \text{Work})^{10},$$

which would in turn imply that the computational cost for reaching an accuracy TOL is expected to be asymptotically $\mathcal{O}(\text{TOL}^{-1/4})$ up to logarithmic terms.

We report computational results in Figure 6-left. In this plot, we show in the horizontal axis the tolerance, TOL, used in the stopping criterion of each algorithm and in the vertical axis the recorded computational time: thus, the flatter the convergence curve, the more effective the method, i.e., moving to smaller tolerance does not require a dramatic increase in the computational time. Of course, the implicit assumption behind this plot is that error actually achieved once the algorithm stops is similar in size to the tolerance enforced as stopping criterion. For MLMC and MIMC, this is guaranteed with “high probability” by the choice of number of samples per mesh, while for MISC we employ the criterion in (16); see Figure 6-right for the effectiveness of these stopping criteria.

We observe from the numerical results that the convergence rates of MLMC and MIMC are roughly 2, in agreement with the theory discussed above. Observe also that the performances of MLMC and MISC are very close, due to the fact that the convergence of the IGA approximation of the physical problem is very fast ($r_i = 4$), hence there is not much advantage in sampling the physical problem over anisotropic meshes in space. MISC features instead a convergence rate of roughly 1/4 as discussed above, after a substantial preasymptotic regime which was also expected. Moreover, MISC features a significantly smaller error, which testifies its superior performance with respect to the other methods reported, in agreement with the previous numerical investigations reported in [11, 12].

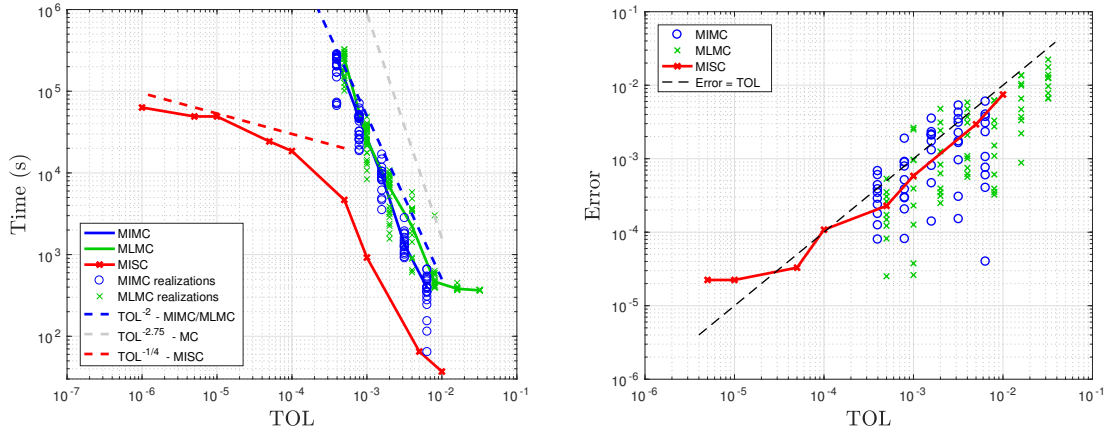


Figure 6: Test 1. Left: convergence results. Right: consistency of stopping criterion; the error has been computed against a sufficiently refined MISC solution. Markers for MLMC and MIMC show the value of the error attained for each method run; we have enforced for MLMC and MIMC that the error should be less than TOL with 95% probability (asymptotically).

5.2. Test 2 - 3d linear elasticity PDE with uncertain Lamé parameters

In this test we consider a slightly more complex problem than in the previous test, i.e., a linear elastic equation, whose strong form reads

$$\begin{cases} -\operatorname{div}[\sigma(\mathbf{u}(\mathbf{x}, \mathbf{y}))] = \mathbf{f}(\mathbf{x}) & \mathbf{x} \in \mathcal{B}, \\ \mathbf{u}(\mathbf{x}, \mathbf{y}) = 0 & \mathbf{x} \in \partial\mathcal{B}_{\text{clamped}}, \\ \sigma(\mathbf{u}(\mathbf{x}, \mathbf{y})) \cdot \mathbf{n} = 0 & \mathbf{x} \in \partial\mathcal{B}_{\text{free}}. \end{cases}$$

Although still elliptic in nature, this problem is computationally more demanding than the previous case as the unknown is now the tri-dimensional displacement field $\mathbf{u} : \mathcal{B} \rightarrow \mathbb{R}^3$. The quantity $\sigma(\mathbf{u}(\mathbf{x}, \mathbf{y}))$ is the Cauchy stress tensor which, upon assuming that the body is undergoing small deformations, can be related to the displacement \mathbf{u} as

$$\sigma(\mathbf{u}(\mathbf{x}, \mathbf{y})) = 2\mu(\mathbf{y}) \frac{\nabla \mathbf{u} + [\nabla \mathbf{u}]^T}{2} + \lambda(\mathbf{y}) \operatorname{div}(\mathbf{u}) I,$$

where μ , λ are the so-called Lamé constants and $I \in \mathbb{R}^{3 \times 3}$ is the identity matrix. In this test, the Lamé constants are assumed to be random variables and model imperfect knowledge of the mechanical properties of the material. One notable practical example in which this might occur is 3d-printing, where the printer manufacturer guarantees such properties only within a confidence range.¹ In our experiments, we thus consider typical value ranges for Titanium in the context of 3d-printing; more specifically, we consider the following ranges for the Young's modulus E and the Poisson's ratio ν ,

$$E \sim \mathcal{U}(105 \times 10^9 \text{ Pa}, 120 \times 10^9 \text{ Pa}), \quad \nu \sim \mathcal{U}(0.265, 0.34),$$

and then link these to the Lamé parameters by the well-known equations

$$\mu = \frac{E}{2(1 + \nu)}, \quad \lambda = \frac{E\nu}{(1 + \nu)(1 - 2\nu)};$$

finally, we let $y_1, y_2 \sim \mathcal{U}([-1, 1])$, and $y_1 \rightarrow E$, $y_2 \rightarrow \nu$ by linear maps. We consider as computational domain \mathcal{B} the “horse-shoe” domain in Figure 7-left: the bottom end $z = 0$ is kept fixed ($\mathcal{B}_{\text{clamped}}$ in the equation) and the rest of the body is free of any constraints ($\mathcal{B}_{\text{free}}$ in the equation). The body is pulled

¹See e.g. <https://www.eos.info/material-m>

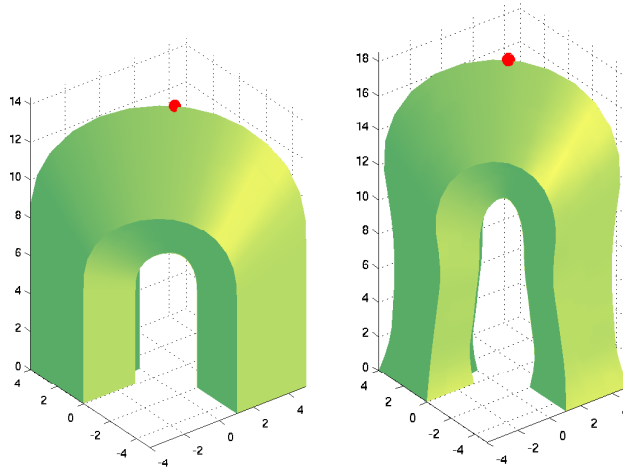


Figure 7: Test 2. Left: undeformed geometry with \mathbf{Q} marked by a red dot. Right: deformation for a random value of the Lamè parameters.

upward by a vertical force $\mathbf{f} = [0, 0, 10^6]$ N/m³, and we are interested at computing the expected elongation measured at \mathbf{Q} , the point marked by a red dot in Figure 7-left, i.e., $\Phi(\mathbf{u}) = \mathbf{u}(\mathbf{Q})$; an example of deformation obtained by two random values of the Lamè parameters is shown in Figure 7-right (magnified by a factor suitable to make it visible in a plot). It is straightforward to see that the problem is well-posed for ρ -almost every $\mathbf{y} \in \Gamma$ in the vector-valued Hilbert space $V = [H^1(\mathcal{B})]^3$. The IGA solver is again set to use NURBS of degree $p = 2$ with maximal continuity² and power-law-scaled knots in the parametric domain as in Test 1. The rates r_i, c_i have been assessed numerically as $r_i = [2.5, 2.5, 2.5]$, $c_1 = [1, 1, 1]$, implying convergence $\mathcal{O}(\text{TOL}^{-2})$ for MIMC and MLMC, $\mathcal{O}(\text{TOL}^{-3})$ for Monte Carlo and $\mathcal{O}(\text{TOL}^{-0.4})$ up to preasymptotic and logarithmic terms for MISC. Results are shown in Figure 8, and again confirm the predicted rates and show that MISC is significantly better than MIMC. We omit convergence results for MLMC, which, as in the previous test, is expected to convergence with a trend analogous to MIMC.

We conclude the discussion on this test by mentioning in-passing that in a sense we are artificially increasing the complexity of the problem by using the Lamè parameters instead of the Young's Modulus and Poisson's ratio. Indeed, since both Lamé constants depend linearly on the Young Modulus E , the solution is inversely proportional to E , given the linearity of the PDE at hand. Thus, $\phi(E, \nu) = 1/E \times \phi^*(\nu)$ and therefore the MISC algorithm could be used over 4 indices (3 in space and 1 for ν) instead of 5. Nonetheless, we choose the formulation with 5 indices because our goal is to showcase the computational efficiency of MISC on high-dimensional problems.

6. Conclusions

In this paper we have shown how to apply the MISC methodology for solving elliptic PDEs with random coefficients to non-square domains by using Isogeometric Analysis (IGA) solvers, which fit perfectly in the MISC framework due to their tensor-structure construction. Observe that in principle any other tensor method able to deal with non-square geometries in a tensorized fashion, such as Finite Differences, Finite Volumes, and \mathbb{Q}^k finite element on hexahedral meshes could be used as well. We have shown the effectiveness of MISC-IGA on a few numerical test cases. Future research directions currently under investigations which very conveniently could be approached with MISC with IGA are:

²actually, everywhere but along the ridge of the horseshoe

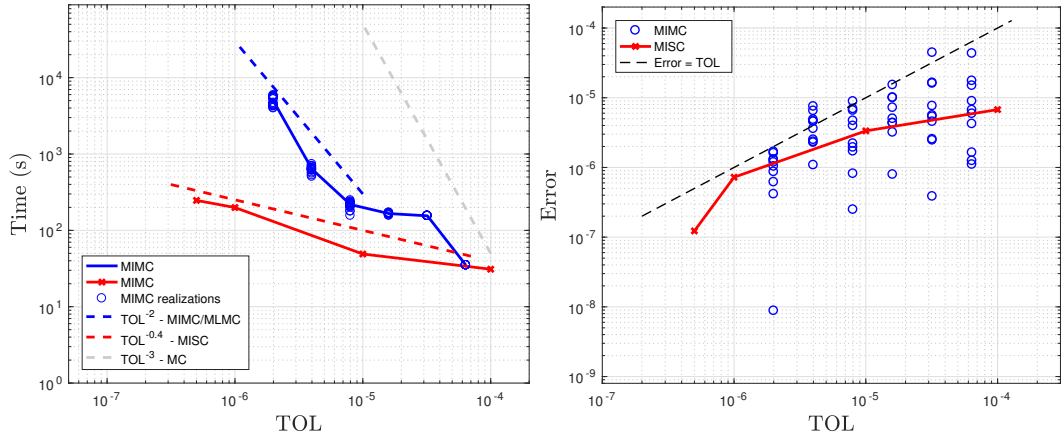


Figure 8: Test 2, computational results. Left: convergence results. Right: consistency of stopping criterion; the error has been computed against a sufficiently refined MISC solution.

- forward UQ problems on domains with uncertain shape (and as a further step, shape optimization under uncertainty): indeed, the B-splines/NURBS representation of a geometry allows to describe deviations from a nominal domain in a very straightforward manner.
- UQ problems defined on unions of disjoint subdomains (or “patches”, in the IGA literature). In this case, MISC could be exploited by allowing the algorithm to choose different meshes in each subdomain, resulting in anisotropic meshes that would refine only a few of the subdomains. The resolution of the PDE on the corresponding non-conformal meshes could be performed by resorting to e.g. Lagrange multipliers [52, 53, 54] or discontinuous Galerkin methods [55, 56, 57] to enforce continuity at the interfaces of the subdomains.

Acknowledgement

The authors would like to thank the Isaac Newton Institute for Mathematical Sciences, Cambridge, for support and hospitality during the programme “Uncertainty quantification for complex systems: theory and methodologies” supported by EPSRC grant no EP/K032208/1, where work on this paper was undertaken. Part of this research has been carried out while the authors visited the Banff International Research Station for Mathematical Innovation and Discovery (BIRS), for the workshop “Computational Uncertainty Quantification” in October 2017,³ organized by Serge Prudhomme, Roger Ghanem, Mohammad Motamed, and Raúl Tempone. The hospitality and support of BIRS is acknowledged with gratitude. This work was supported by the KAUST Office of Sponsored Research (OSR) under award numbers URF/1/2281-01-01 and URF/1/2584-01-01 in the KAUST Competitive Research Grants Program-Round 3 and 4, respectively. Lorenzo Tamellini also received support from the European Unions Horizon 2020 research and innovation program through the grant no. 680448 “CAxMan”, and by the GNCS 2018 project “Metodi non conformi per equazioni alle derivate parziali”.

References

- [1] R. Ghanem, D. Higdon, H. Owhadi, Handbook of Uncertainty Quantification, Handbook of Uncertainty Quantification, Springer International Publishing, 2016.
- [2] T. Sullivan, Introduction to Uncertainty Quantification, Texts in Applied Mathematics, Springer International Publishing, 2015.

³<https://www.birs.ca/events/2017/5-day-workshops/17w5072>

- [3] R. Smith, *Uncertainty Quantification: Theory, Implementation, and Applications*, Computational Science and Engineering, Society for Industrial and Applied Mathematics, 2013.
- [4] F. Nobile, R. Tempone, C. Webster, An anisotropic sparse grid stochastic collocation method for partial differential equations with random input data, *SIAM J. Numer. Anal.* 46 (5) (2008) 2411–2442.
- [5] F. Nobile, L. Tamellini, R. Tempone, Convergence of quasi-optimal sparse-grid approximation of Hilbert-space-valued functions: application to random elliptic PDEs, *Numerische Mathematik* 134 (2) (2016) 343–388.
- [6] A. Cohen, R. Devore, C. Schwab, Analytic regularity and polynomial approximation of parametric and stochastic elliptic PDE'S, *Anal. Appl. (Singap.)* 9 (1) (2011) 11–47.
- [7] A. Chkifa, A. Cohen, R. Devore, C. Schwab, Sparse adaptive Taylor approximation algorithms for parametric and stochastic elliptic PDEs, *ESAIM: Mathematical Modelling and Numerical Analysis* 47 (1) (2013) 253–280.
- [8] K. Cliffe, M. Giles, R. Scheichl, A. Teckentrup, Multilevel monte carlo methods and applications to elliptic pdes with random coefficients, *Computing and Visualization in Science* 14 (1) (2011) 3–15.
- [9] A.-L. Haji-Ali, F. Nobile, R. Tempone, Multi-index Monte Carlo: when sparsity meets sampling, *Numerische Mathematik* (2015) 1–40.
- [10] B. Peherstorfer, K. Willcox, M. Gunzburger, Survey of multifidelity methods in uncertainty propagation, inference, and optimization, *SIAM Review* 60 (3) (2018) 550–591.
- [11] A. Haji-Ali, F. Nobile, L. Tamellini, R. Tempone, Multi-index stochastic collocation for random {PDEs}, *Computer Methods in Applied Mechanics and Engineering* 306 (2016) 95 – 122.
- [12] A.-L. Haji-Ali, F. Nobile, L. Tamellini, R. Tempone, Multi-index Stochastic Collocation convergence rates for random PDEs with parametric regularity, *Foundations of Computational Mathematics* 16 (6) (2016) 1555–1605.
- [13] H.-J. Bungartz, M. Griebel, D. Röschke, C. Zenger, Pointwise convergence of the combination technique for the Laplace equation, *East-West J. Numer. Math.* 2 (1994) 21–45.
- [14] H. Bungartz, M. Griebel, Sparse grids, *Acta Numer.* 13 (2004) 147–269.
- [15] M. Griebel, M. Schneider, C. Zenger, A combination technique for the solution of sparse grid problems, in: P. de Groen, R. Beauwens (Eds.), *Iterative Methods in Linear Algebra*, IMACS, Elsevier, North Holland, 1992, pp. 263–281.
- [16] M. Hegland, J. Garcke, V. Challis, The combination technique and some generalisations, *Linear Algebra and its Applications* 420 (23) (2007) 249 – 275.
- [17] S. Smolyak, Quadrature and interpolation formulas for tensor products of certain classes of functions, *Dokl. Akad. Nauk SSSR* 4 (1963) 240–243.
- [18] V. Barthelmann, E. Novak, K. Ritter, High dimensional polynomial interpolation on sparse grids, *Adv. Comput. Math.* 12 (4) (2000) 273–288.
- [19] A. L. Teckentrup, P. Jantsch, C. G. Webster, M. Gunzburger, A Multilevel Stochastic Collocation Method for Partial Differential Equations with Random Input Data, *SIAM/ASA Journal on Uncertainty Quantification* 3 (1) (2015) 1046–1074.
- [20] H. W. van Wyk, Multilevel sparse grid methods for elliptic partial differential equations with random coefficients, arXiv arXiv:1404.0963, e-print (2014).
- [21] H. Harbrecht, M. Peters, M. Siebenmorgen, On multilevel quadrature for elliptic stochastic partial differential equations, in: *Sparse Grids and Applications*, Vol. 88 of *Lecture Notes in Computational Science and Engineering*, Springer, 2013, pp. 161–179.
- [22] I. Babuška, F. Nobile, R. Tempone, A stochastic collocation method for elliptic partial differential equations with random input data, *SIAM Review* 52 (2) (2010) 317–355.
- [23] D. Xiu, J. Hesthaven, High-order collocation methods for differential equations with random inputs, *SIAM J. Sci. Comput.* 27 (3) (2005) 1118–1139.
- [24] T. J. R. Hughes, J. A. Cottrell, Y. Bazilevs, Isogeometric analysis: CAD, finite elements, NURBS, exact geometry and mesh refinement, *Computer Methods in Applied Mechanics and Engineering* 194 (39) (2005) 4135–4195.
- [25] J. A. Cottrell, T. J. R. Hughes, Y. Bazilevs, *Isogeometric Analysis: toward integration of CAD and FEA*, John Wiley & Sons, 2009.
- [26] L. Beirao Da Veiga, A. Buffa, G. Sangalli, R. Vázquez, Mathematical analysis of variational isogeometric methods, *Acta Numerica* 23 (2014) 157–287.
- [27] J. Beck, G. Sangalli, L. Tamellini, A sparse-grid isogeometric solver, *Computer Methods in Applied Mechanics and Engineering* 335 (–) (2018) 128–151.
- [28] M. Montardini, G. Sangalli, L. Tamellini, Optimal-order isogeometric collocation at Galerkin superconvergent points, *Computer Methods in Applied Mechanics and Engineering*.
- [29] H. Gomez, L. De Lorenzis, The variational collocation method, *Computer Methods in Applied Mechanics and Engineering* 309 (2016) 152–181.
- [30] C. Anitescu, Y. Jia, Y. J. Zhang, T. Rabczuk, An isogeometric collocation method using superconvergent points, *Computer Methods in Applied Mechanics and Engineering* 284 (2015) 1073–1097.
- [31] H. Casquero, L. Liu, Y. Zhang, A. Reali, H. Gomez, Isogeometric collocation using analysis-suitable t-splines of arbitrary degree, *Computer Methods in Applied Mechanics and Engineering* 301 (2016) 164–186.
- [32] O. G. Ernst, B. Sprungk, L. Tamellini, Convergence of Sparse Collocation for Functions of Countably Many Gaussian Random Variables (with Application to Lognormal Elliptic Diffusion Problems), *SIAM Journal on Numerical Analysis* 56 (2) (2018) 877–905.
- [33] L. N. Trefethen, Is Gauss quadrature better than Clenshaw-Curtis?, *SIAM Rev.* 50 (1) (2008) 67–87.
- [34] F. Nobile, L. Tamellini, R. Tempone, Comparison of Clenshaw-Curtis and Leja Quasi-Optimal Sparse Grids for the Approximation of Random PDEs, in: R. M. Kirby, M. Berzins, J. S. Hesthaven (Eds.), *Spectral and High Order Methods for*

- Partial Differential Equations - ICOSAHOM '14, Vol. 106 of Lecture Notes in Computational Science and Engineering, Springer International Publishing, 2015, pp. 475–482.
- [35] A. Narayan, J. D. Jakeman, Adaptive Leja Sparse Grid Constructions for Stochastic Collocation and High-Dimensional Approximation, *SIAM Journal on Scientific Computing* 36 (6) (2014) A2952–A2983.
 - [36] A. Chkifa, On the Lebesgue constant of Leja sequences for the complex unit disk and of their real projection, *Journal of Approximation Theory* 166 (0) (2013) 176 – 200.
 - [37] J. Bäck, F. Nobile, L. Tamellini, R. Tempone, Stochastic spectral Galerkin and collocation methods for PDEs with random coefficients: a numerical comparison, in: *Spectral and High Order Methods for Partial Differential Equations*, Vol. 76 of Lecture Notes in Computational Science and Engineering, Springer, 2011, pp. 43–62.
 - [38] M. Bieri, A sparse composite collocation finite element method for elliptic spdes., *SIAM Journal on Numerical Analysis* 49 (6) (2011) 2277–2301.
 - [39] T. Gerstner, M. Griebel, Dimension-adaptive tensor-product quadrature, *Computing* 71 (1) (2003) 65–87.
 - [40] C. Schillings, C. Schwab, Sparse, adaptive Smolyak quadratures for Bayesian inverse problems, *Inverse Problems* 29 (6).
 - [41] F. Nobile, L. Tamellini, F. Tesei, R. Tempone, An adaptive sparse grid algorithm for elliptic PDEs with lognormal diffusion coefficient, in: J. Garcke, D. Pflüger (Eds.), *Sparse Grids and Applications – Stuttgart 2014*, Vol. 109 of Lecture Notes in Computational Science and Engineering, Springer International Publishing Switzerland, 2016, pp. 191–220.
 - [42] B. Guo, I. Babuška, The h-p version of the finite element method, *Computational Mechanics* 1 (3) (1986) 203–220.
 - [43] I. Babuška, T. Strouboulis, *The finite element method and its reliability*, Numerical Mathematics and Scientific Computation, The Clarendon Press Oxford University Press, New York, 2001.
 - [44] D. Schillinger, J. Evans, A. Reali, M. Scott, T. Hughes, Isogeometric collocation: cost comparison with Galerkin methods and extension to adaptive hierarchical NURBS discretizations, *Comput. Methods Appl. Mech. Engrg.* 267 (2013) 170 – 232.
 - [45] D. S. Guignard, F. Nobile, A posteriori error estimation for the stochastic collocation finite element method, *Mathicse Report nr 24.2017*.
 - [46] R. Vazquez, A new design for the implementation of isogeometric analysis in octave and matlab: Geopdes 3.0, *Computers & Mathematics with Applications* 72 (3) (2016) 523 – 554.
 - [47] A. Cohen, R. DeVore, Approximation of high-dimensional parametric pdes, *Acta Numerica* 24 (2015) 1159.
 - [48] J. Beck, F. Nobile, L. Tamellini, R. Tempone, A Quasi-optimal Sparse Grids Procedure for Groundwater Flows, in: *Spectral and High Order Methods for Partial Differential Equations - ICOSAHOM 2012*, Vol. 95 of Lecture Notes in Computational Science and Engineering, Springer, 2014, pp. 1–16.
 - [49] R. G. Ghanem, P. D. Spanos, *Stochastic finite elements: a spectral approach*, Springer-Verlag, New York, 1991.
 - [50] A. Chkifa, A. Cohen, C. Schwab, Breaking the curse of dimensionality in sparse polynomial approximation of parametric PDEs, *Journal de Mathématiques Pures et Appliquées* 103 (2) (2015) 400 – 428.
 - [51] N. Collier, A. Haji-Ali, F. Nobile, E. von Schwerin, R. Tempone, A continuation multilevel monte carlo algorithm, *BIT Numerical Mathematics* (2014) 1–34.
 - [52] E. Brivadis, A. Buffa, B. Wohlmuth, L. Wunderlich, Isogeometric mortar methods, *Computer Methods in Applied Mechanics and Engineering* 284 (2015) 292 – 319, isogeometric Analysis Special Issue.
 - [53] C. Hesch, P. Betsch, Isogeometric analysis and domain decomposition methods, *Computer Methods in Applied Mechanics and Engineering* 213216 (2012) 104 – 112.
 - [54] Í. Temizer, P. Wriggers, T. Hughes, Three-dimensional mortar-based frictional contact treatment in isogeometric analysis with NURBS, *Comput. Methods Appl. Mech. Engrg.* 209–212 (2012) 115 – 128.
 - [55] P. Antonietti, I. Mazzieri, A. Quarteroni, F. Rapetti, Non-conforming high order approximations of the elastodynamics equation, *Computer Methods in Applied Mechanics and Engineering* 209212 (2012) 212 – 238.
 - [56] J. Nitsche, Über ein Variationsprinzip zur Lösung von Dirichlet-Problemen bei Verwendung von Teilräumen, die keinen Randbedingungen unterworfen sind, *Abh. Math. Sem. Univ. Hamburg* 36 (1971) 9–15, collection of articles dedicated to Lothar Collatz on his sixtieth birthday.
 - [57] D. N. Arnold, F. Brezzi, B. Cockburn, L. D. Marini, Unified analysis of discontinuous galerkin methods for elliptic problems, *SIAM Journal on Numerical Analysis* 39 (5) (2002) 1749–1779. doi:10.1137/S0036142901384162.